

Design and demonstration of PECVD multilayer dielectric mirrors optimized for micromachined cavity angled sidewalls[☆]

Maximillian A. Perez^{a,*}, John Kitching^b, Andrei M. Shkel^a

^a MicroSystems Laboratory, University of California, Irvine, CA 92697-3975, USA

^b Time and Frequency Division, National Institute of Standards and Technology, Boulder, CO 80305-3328, USA

ARTICLE INFO

Article history:

Received 16 July 2008

Accepted 13 October 2008

Available online 25 October 2008

PACS:

07.07.Df

33.25.+k

42.79.Fm

42.82.Bq

85.85.+j

Keywords:

Atomic MEMS

Bragg reflector

Optical MEMS

PECVD

Thin films

Vapor cells

ABSTRACT

This paper reports on the design and implementation of high efficiency, nonmetallic reflectors integrated on the sidewalls of micromachined cavities. Due to shadowing from deposition within a cavity, significant variation in the thicknesses of the dielectric thin films composing the reflectors are encountered when the layers are deposited by Plasma Enhanced Chemical Vapor Deposition (PECVD). These gradients in thickness limit the performance of the reflector at the intended design wavelength. An optimized design procedure is described to maximize the performance of the reflector at the D_1 absorption wavelength of ^{87}Rb of 795 nm for use in micromachined atomic vapor cells. The reflector design is based on multiple shifted quarter wave Bragg reflectors in series, which extends the reflective bandwidth for increased robustness to film thickness gradients. The extended reflectance range maintains high reflection at the design wavelength despite greater than 70% decrease in film thickness across the reflector surface. The reflector technology is ideally suited for use in atomic MEMS vapor cell applications by achieving high reflectance while maintaining light polarization. We demonstrate less than 2 dB of return loss with circular polarization ellipticity maintained to $\pm 2^\circ$.

© 2008 Elsevier B.V. All rights reserved.

1. Introduction

Miniature vapor cells for emerging atomic MEMS applications, such as chip scale atomic clocks [1], magnetometers [2,3] and gyroscopes, depend on the efficient routing of laser light by use of micromachined reflectors. Cells containing rubidium alkali vapor need low reflection losses at the ^{87}Rb D_1 transition wavelength of 795 nm after multiple reflections inside the vapor cell cavity formed in bulk micromachined wet-etched silicon, as shown in Fig. 1. Vapor cells designs with integrated reflectors enable the implementation of compact atomic MEMS systems. For instance, the vapor cell probe beam may be emitted by a vertical cavity surface emitting laser (VCSEL) and interrogated by a photocollector such that both opto-

electronic components are integrated as discrete components on a single electronics plane.

However, uncoated silicon is not sufficiently reflective for use as a high performance mirror, as it loses more than 2/3 of incident optical energy in bulk transmission. Previously, rubidium vapor cells with optical return performance superior to uncoated silicon have been demonstrated by use of multilayer dielectric reflectors integrated on the sidewalls of wet-etched silicon cavities fabricated by use of Plasma Enhanced Chemical Vapor Deposition (PECVD) [4]. Although these reflectors have the potential to reflect light with negligible loss, large variations in the thin film thicknesses were observed due to the deposition technology that limited the reflector performance.

PECVD has many practical advantages over other thin film fabrication methods, such as Physical Vapor Deposition (PVD), including higher deposition rates and the formation of films with better mechanical and environmental robustness [5]. However, the thicknesses of PECVD fabricated thin films deposited onto the sidewalls of micromachined cavities rapidly decrease with cavity depth. This film thinning is due to the decrease in the arrival angle available to reactant species (shadowing) from the PECVD reactor chamber [6]. Previously, the effects of such film thinning has been observed

[☆] This paper is part of the Special Section of the Micromechanics Section of Sensors and Actuators based on contributions revised from the Technical Digest of the 2008 Solid-State Sensors, Actuators and Microsystems Workshop sponsored by the Transducer Research Foundation, Inc. (1–5 June 2008, Hilton Head Island, South Carolina, USA).

* Corresponding author. Tel.: +1 949 824 6314.

E-mail address: max.perez@uci.edu (M.A. Perez).

URL: <http://www.mems.eng.uci.edu> (M.A. Perez).

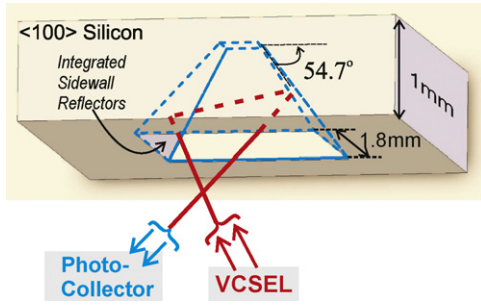


Fig. 1. Bulk micromachined vapor cell with integrated reflectors for atomic MEMS.

on multilayer reflectors deposited on shallowly etched substrate facets intended for use with integrated optoelectronic components [7]. However, reflectors integrated into deeply etched cavities, such as required for atomic MEMS vapor cells, present significant challenges in maintaining reflector uniformity when PECVD is used. For the vapor cell geometry previously proposed in [4], the nonuniformity represents a reduction in layer thickness by more than 70% from the top to the bottom of all of the faces of the cavity sidewalls. The film nonuniformity results in an optical shift of the reflection spectrum of the integrated Bragg reflector to wavelengths below the design wavelength. In this work, a thin film reflector design methodology is described and demonstrated that maintains high reflectance at the design wavelength in the presence of these challenging deposition conditions.

An example of one such optimized reflector deposited on the angled sidewalls of a wet bulk micromachined cavity is shown in Fig. 2. When the multilayer reflector is deposited on the angled cavity sidewalls, thinning of the film from top to bottom of the cell results in a shift in the reflection to lower wavelengths. The reflectance shift is visible to the naked eye by the color change of the reflector face from red to yellow to blue down the sidewall face. In conventional Bragg reflector designs, since the optimum reflectance wavelength varies over the area of the reflector, the efficiency at the design wavelength is compromised.

In the case shown in Fig. 2, an advanced thin film reflector design is applied to extend the range of the high reflectance band, and the deposition process is optimizing for the intended application wavelength. This design and fabrication process maximizes the reflectance down the cavity sidewall at the design wavelength.

This paper describes the design and demonstrates the potential of PECVD reflectors for integration onto the sidewalls of micro-machined cavities for atomic MEMS applications. This work is an expansion of the preliminary results presented at the 2008 Hilton Head Solid-State Sensors, Actuators and Microsystems Workshop

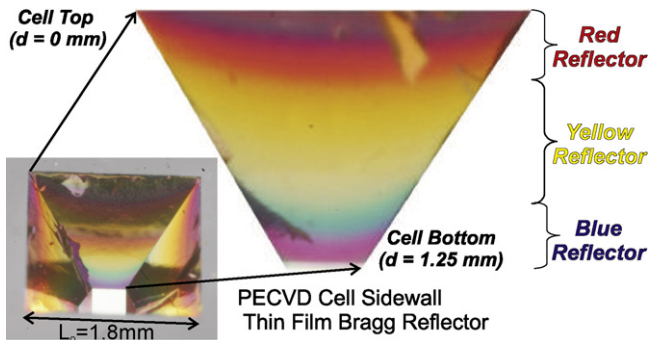


Fig. 2. Optimized extended 12 layer ($6 \times |\alpha\text{SiSiO}_2|$) PECVD Bragg reflector on the sidewall of a reflector cell with shifting wavelength reflectance (red to yellow to blue) due to deposition nonuniformity. (For interpretation of the references to color in this figure legend, the reader is referred to the web version of the article.)

[8]. In Section 2, the design of sidewall integrated Bragg reflectors is presented. This section includes the effects of cavity shadowing, optimized design for sidewall integration, the use of the reflector bandwidth to estimate robustness to thinning of the reflector films and the design of Bragg reflectors with extended reflectance bandwidth. Section 3 models the response of both conventional and extended bandwidth reflector designs when integrated on a cavity sidewall and compares the performance. Section 4 describes the specific implementation of the cavity sidewall integrated extended Bragg reflector. Finally, in Section 5 the reflector bandwidth of the extended Bragg reflector is characterized and compared to that of a conventional Bragg reflector, and the performance of the extended Bragg reflector design is evaluated for single and multiple reflections within a reflector cell.

2. Design of PECVD multilayer reflectors for cavity sidewalls

2.1. Bragg reflector bandwidth

The design of micromachined cells with integrated Bragg reflectors for rubidium vapor cells has been previously described in [4]. Briefly, the light reflected at the interface between each layer may be made to constructively interfere to maximize the total reflected optical power at a specific wavelength. The reflectivity is maximized if the structure is composed of alternating thin film layers each of optical thickness equal to one-quarter wavelength of the light to be reflected, as given by [9]

$$t = \frac{\lambda_0}{4n}, \quad (1)$$

where t is the thickness of each layer, λ_0 is the wavelength of light to be reflected and n is the index of refraction of each layer.

The high reflectance wavelength bandwidth is given by [9]

$$2\Delta g = \frac{4}{\pi} \sin^{-1} \left(\frac{n_H/n_L - 1}{n_H/n_L + 1} \right), \quad (2)$$

where g is the normalized wavenumber ($g = \lambda_0/\lambda$) and n_H is the higher and n_L the lower index of refraction of each of the thin film materials. The wavelengths at the upper (λ_+) and lower (λ_-) limits of this reflectance band are given by

$$\lambda_+ = \frac{\lambda_0}{1 - \Delta g} \quad (3)$$

for the wavelength at the upper limit and

$$\lambda_- = \frac{\lambda_0}{1 + \Delta g}, \quad (4)$$

for the wavelength at the lower limit, which yields the reflector bandwidth $\Delta\lambda$ in wavelength units given by

$$\Delta\lambda = \lambda_+ - \lambda_- = \frac{2\Delta g}{1 - (\Delta g)^2} \lambda_0. \quad (5)$$

The effect of increased index of refraction contrast n_H/n_L between the thin film pairs $|n_H n_L|$ on (2) and (5) are shown in Fig. 3. For low contrast materials, the normalized reflector bandwidths expressed by $2\Delta g$ and $\Delta\lambda/\lambda_0$ are numerically identical. However, for reflectors formed with high contrast materials, the differences become significant (10% at $n_H/n_L = 2.7$). Overlaid are the expected reflector bandwidth that may be obtained with thin film materials readily deposited using PECVD, as tabulated in Table 1. It may be readily observed that the width of the reflectance band is maximized by use of high contrast ratio materials.

Amorphous silicon (αSi) and silicon dioxide (SiO_2) yield the highest optical index contrast available ($n_H/n_L = 2.7$, $\Delta g = 0.3$), such that for $\lambda_0 = 795 \text{ nm}$, $\Delta\lambda = 520 \text{ nm}$. Reflector bandwidth of integrated cavity sidewall reflectors as wide as $\Delta\lambda = 500 \text{ nm}$ has

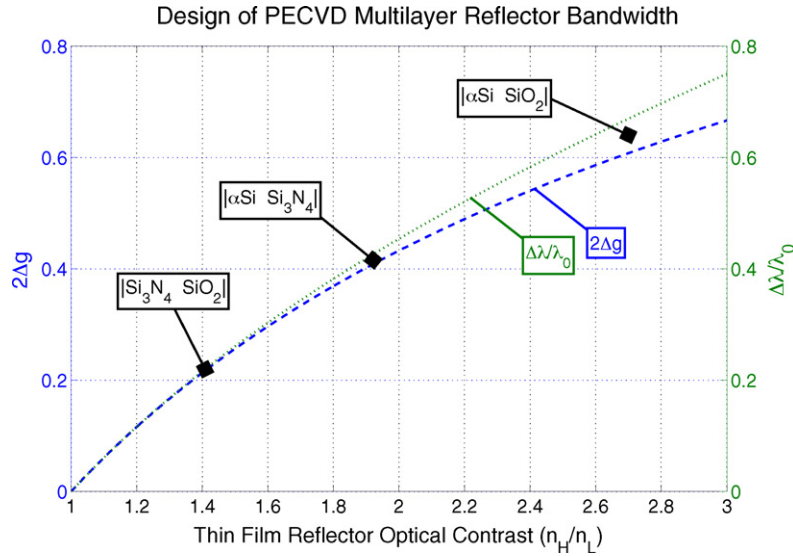


Fig. 3. Reflector bandwidth available for multilayer dielectric reflectors formed from pairs of commonly available PECVD materials: amorphous silicon (αSi), silicon nitride (Si_3N_4), and silicon dioxide (SiO_2)

been observed. In addition to wide bandwidths, high optical contrast allows high reflectances to be achieved while the total number of required layers is minimized. An ideal $|\alpha\text{SiSiO}_2|$ multilayer reflector has the potential to reach a reflectance of 99% with only three layer pairs or six total thin film layers [4].

The reflective efficiency of $|\alpha\text{SiSiO}_2|$ multilayer reflectors is limited by absorption in the αSi layers due to the non-negligible coefficient of extinction αSi at wavelengths approaching the visible light spectrum. These reflectance losses may be shown to be limited to less than 6.2% [11]. The negligible coefficients of extinction in $|\text{Si}_3\text{N}_4\text{SiO}_2|$ multilayer reflectors make these materials preferable for light approaching the visible wavelengths but require more than 12 layers to approach reflectances over 90%. In addition, the limited reflectance bandwidth leaves such reflectors vulnerable to variations in the reflector thickness [4].

2.2. PECVD cavity shadowing

Shown previously in [4], PECVD films deposited onto the sidewalls of etched cavities are not uniform and decrease with the depth into the trench. The thin film deposition rate into a cavity is characterized by the arrival angles opposite (θ) and parallel (ϕ) to the deposition face open to the PECVD reactor vessel, as defined in Fig. 4.

Fig. 4 shows the two orthogonal arrival angles both between the deposition face and the opposite wall (θ) and between the two adjacent walls (ϕ). The deposition face has a wet-etch angle α . Arrival angle θ may be calculated by

$$\theta = \sin^{-1} \left\{ \sqrt{\frac{L_0^2 \sin^2(\alpha)}{L_0^2 + d^2 - 2L_0d \cos(\alpha)}} \right\}, \quad (6)$$

Table 1
Optical properties of selected PECVD materials at $\lambda = 795 \text{ nm}$.

Film material	Index of refraction (n)	Coefficient of extinction (k)	Ref.
αSi	3.9	0.13	[10]
Si_3N_4	2.0	$< 2.2 \times 10^{-4}$	[10]
SiO_2	1.45	$< 4.5 \times 10^{-6}$	[10]

where d is the depth along the sidewall face, L_0 is the cavity opening width, α is the etch angle, and the oblique or acute angle solution for $\sin^{-1}\{\cdot\}$ must be chosen to provide the physically suitable and continuous solution as a function of sidewall depth.

The geometric dependency of arrival angle ϕ may be extended from that presented in [4] to include shadowing effects at points off the sidewall centerline. The angle ϕ may then be calculated across the sidewall area by

$$\phi = \tan^{-1} \left\{ \frac{L_0/2 + x}{d} \right\} + \tan^{-1} \left\{ \frac{L_0/2 - x}{d} \right\}, \quad (7)$$

where x is the horizontal displacement from the sidewall centerline. Expression (7) collapses to $\phi = 2 \tan^{-1}(L_0/2d)$ along the sidewall centerline, which for $L_0/d \ll 1$ is the same as the approximate $\phi = \tan^{-1}\{L_0/d\}$ deposition thickness dependence presented by Adams for vertical sidewalls [6].

The product of the two arrival angles may be used to estimate the total effect of arrival angle shadowing. When normalized by the arrival angles available to a planar substrate ($\theta_{\perp} = \pi$, $\phi_{\perp} = \pi$), the fractional change in the arrival angle may be used to estimate the change in the deposition rate onto a micromachined cavity sidewall from that onto a planar surface. This yields the ratio of thickness of a thin film on a cavity sidewall to the thickness on a planar surface

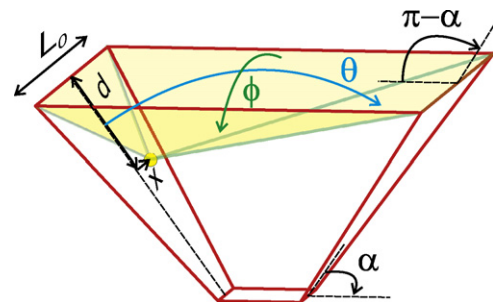


Fig. 4. Orthogonal arrival angles (θ , ϕ) for deposition along the sidewall centerline of a symmetric bulk micromachined cavity of wet-etch angle α and square etch window of edge length L_0 .

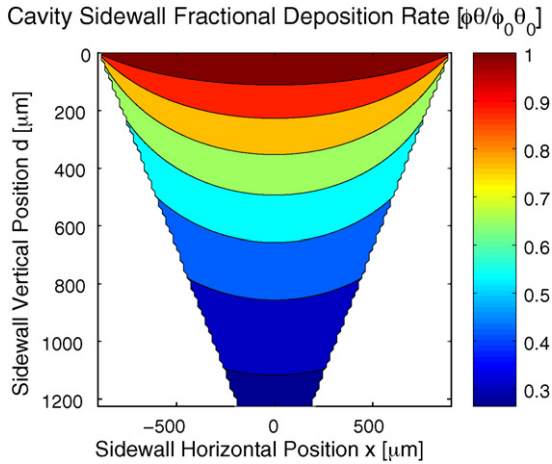


Fig. 5. Deposition rate variation estimated from normalized change in arrival angle product from (10) for a cavity with the geometry of Fig. 4 ($L_0 = 1.8$ mm, $\alpha = 54.7^\circ$).

t_\perp given by

$$\frac{t}{t_\perp} = \frac{\phi\theta}{\phi_\perp\theta_\perp} = \frac{\phi\theta}{\pi^2}. \quad (8)$$

Two thin film deposition characteristics are predicted by this model. A discrete step change in the deposition thin film thickness from perpendicular deposition (t_\perp) to deposition on the top of the sidewall at $d = 0$ (t_0), is such that the fractional change in film thickness is given by

$$\frac{t_0}{t_\perp} = \frac{\phi_0\theta_0}{\phi_\perp\theta_\perp} = \frac{\pi\alpha}{\pi^2}. \quad (9)$$

The effects on reflector design due to the discrete reflectance step shift are addressed through a Bragg reflector design appropriately shifted to maximize the reflectance across the face of the sidewall, as described in Section 2.3.

In addition, a continuous shift in the thin film thickness down the face of the sidewall is expected. When normalized by the thickness at the top of the sidewall at $d = 0$, the fractional thinning may be modeled by

$$\frac{t}{t_0} = \frac{\phi\theta}{\phi_0\theta_0} = \frac{\phi\theta}{\pi\alpha}. \quad (10)$$

The predicted change in deposition rate across the surface of the cavity sidewall due to shadowing for the geometry investigated here is shown in Fig. 5. At the bottom of the sidewall, the film thickness is less than 30% of the thickness at the top of the cavity sidewall. Since the wavelength of maximum reflectance λ_0 of a Bragg reflector is proportional to the film thickness given by (1), the decrease in deposition rate will result in a shift in reflectance to lower wavelengths. This effect is observed in Fig. 2 where the pattern of the color variation observed on the sidewall of the reflector cell is nearly identical to that predicted by the cavity shadowing model in Fig. 5. The complications due to the continuously thinning films on the sidewall reflector require both the optimized design to be described in Section 2.3, as well as an advanced thin film reflector design, to be presented in Section 2.5.

2.3. Optimized Bragg reflector for cavity sidewall integration

PECVD process parameters are generally defined in terms of the planar deposition rates. Since the physical thickness of each layer will shift across the interface from planar to sidewall deposition, it is of interest to define the design wavelength for planar deposition λ_\perp^0 that will achieve a sidewall reflector design at wavelength λ . In

addition, it is desirable to optimize the planar design to maximize the reflectance at λ over as much of the sidewall as possible under the shifts in the reflector to lower wavelengths down the sidewall into the cavity.

The reflector may be optimized at λ if it is equal to the wavelength λ_- at the lower limit of the reflectance band at the top of the cavity sidewall. This technique provides that the entire reflectance band is available for decreasing film thickness and shifts to lower reflectance band wavelengths. Combining (1), (4), and (8) yields

$$\frac{\phi\theta}{\phi_\perp\theta_\perp} = \frac{\lambda_-(1 + \Delta g)}{\lambda_\perp^0}. \quad (11)$$

Optimizing (11) by setting $\lambda = \lambda_-$ and evaluating the left hand side for the shadowing at the top of the sidewall for $d = 0$ using (9) yields

$$\lambda_\perp^0 = \frac{\lambda(1 + \Delta g)}{1 - \alpha/\pi}, \quad (12)$$

where α is measured in radians. Relation (12) is used to determine the planar deposition design wavelength λ_\perp^0 , which yields a reflector designed to maximize the reflectance at a wavelength λ deposited on a sidewall at etch angle α . The wavelength λ_\perp^0 is used to establish the deposition time by use of the thin film thickness from (1) for the deposition rates in any particular PECVD system.

2.4. Robustness to film thinning

The reflection bandwidth may be used as a measure of the robustness to film thinning due to cavity shadowing when used in narrowband (laser) applications at a reflector design wavelength λ . Thinning of the film layer thicknesses will shift the reflection wavelength according to (1). If the variation in thickness causes a shift in the target wavelength λ greater than the bandwidth of the reflector $\Delta\lambda$, the reflectance will be reduced at the target wavelength. Combining (3) and (4) with (1), the reflector wavelength limits over the fractional change in thin film thickness are evaluated according to

$$\frac{t}{t_0} = \frac{(1 - \Delta g)}{(1 + \Delta g)}, \quad (13)$$

where t_0 is the thickness at $d = 0$ and $\lambda \equiv \lambda_- \equiv \lambda_+$ for a reflector ideally optimized to maximize reflectance at λ . For an $|\alpha\text{SiSiO}_2|$ Bragg reflector, $t/t_0 = 0.54$, which indicates that using (12) the reflector may be optimized to be robust for a reduction in the thin film thicknesses of up to 46%.

2.5. Bragg reflectors with extended bandwidth

The variation in film thickness due to cavity shadowing in a particular cavity geometry may be too large to maintain high reflectance at the target wavelength by use of a conventional Bragg reflector, despite optimization. The thinning is predicted by the model presented in Section 2.2 and shown in Fig. 5 for the geometry explored in this work. At the bottom of the sidewall, cavity shadowing will result in a reduction in the thickness of the reflector films of more than 70% and the film thickness will have decreased to less than $t/t_0 = 0.3$. No materials readily deposited by using PECVD will have suitable contrast to be able to form a Bragg reflector of a conventional design with sufficient reflectance bandwidth to provide a stable reflector in the presence of this amount of film thinning.

More advanced thin film reflector designs may be used to extend the reflectance band over a wider spectral region than is available from the optical contrast between any particular pair of thin film materials. A simple design, introduced by Turner and Baumeister in 1966 [12], uses two or more Bragg reflectors of shifted design in series to form extended contiguous high reflectance bands. Oth-

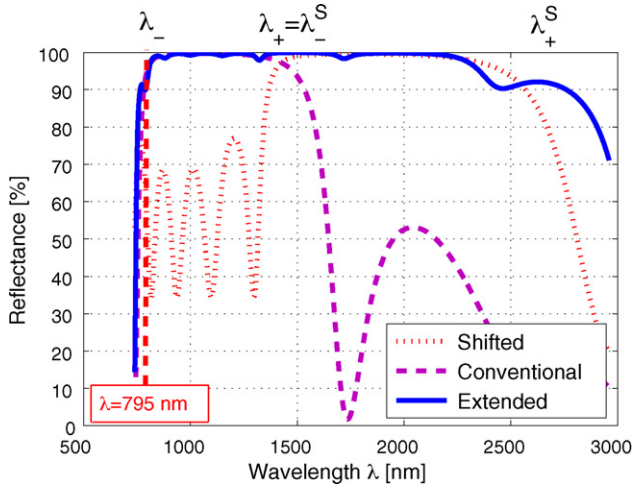


Fig. 6. Extended reflectance band formed from a conventional and shifted Bragg reflector in series.

ers have proposed designs based on the continuous geometric or arithmetic progression of the film thicknesses [13].

By use of the approach of Turner and Baumeister [12], the bandwidth of the reflector can be extended by using two Bragg reflectors in series. The reflectance response of the extended Bragg reflector is shown analytically in Fig. 6. In addition to the conventional Bragg reflector designed according to the optimized procedure introduced in Section 2.3, a second shifted Bragg reflector is deposited. The second reflector provides high reflectance over longer wavelengths and adds to the total reflectance bandwidth. The design wavelength of the second reflector is optimally designed by shifting the design wavelength by the reflectance bandwidth to λ_0^S . Using (3) and (4) yields

$$\frac{\lambda_0^S}{\lambda_0} = \frac{(1 + \Delta g)}{(1 - \Delta g)}, \quad (14)$$

where the upper reflectance band limit of the original reflector is matched to the lower limit of the second reflector ($\lambda_+ \equiv \lambda_-^S$) to create a composite reflector with an ideally extended reflectance of $\Delta g_{Ext} = 2\Delta g$.

By combining (2) with (14), for the Bragg reflector composed of $|\alpha\text{SiSiO}_2|$ layer pairs, the shifted reflector is optimally designed with $\lambda_0^S = 1.8\lambda_0$. From (13) and $\Delta g_{Ext} = 0.6$, the extended reflector is able to maintain high reflectance over thickness reductions due to cavity shadowing down to $t/t_0 = 0.3$. As shown analytically in Fig. 7, the use of an extended band reflector allows elevated reflectance to be maintained down the sidewall for up to 70% thinning due to cavity shadowing. Effects due to dispersion need not be included since only the response at the design wavelength is considered.

3. Sidewall reflector performance: modeling and comparison

In this section, the performance of a Bragg reflector with an extended bandwidth integrated onto the sidewalls of a wet-etched cavity is considered and compared to that of a conventionally designed Bragg reflector. The conventional Bragg reflector and the extended Bragg reflector designs are shown schematically in Fig. 8(a) and (b), respectively. While a conventional Bragg reflector may be optimally designed to maximize the reflector bandwidth over the top portion of the cavity sidewall and to maximize the reflectance at the design wavelength λ between the upper λ_+ and lower limits λ_- of the reflectance bandwidth, the thinning of the films due to deposition shadowing causes the reflector bandwidth

to shift to lower wavelengths and to become transparent to the design wavelength over the lower section of the sidewall. However, the extended Bragg reflector design uses the second, thicker Bragg reflector to provide reflectance at the design wavelength over the lower section of the cavity sidewall.

The optimized conventional reflector is modeled as an ideal dielectric thin film reflector at the design wavelength of $\lambda = 795$ nm for an angle of incidence of $\theta_i = 45^\circ$, and optical losses within the films are not considered. By considering the change in the thickness of the reflector films due to the fractional change in the PECVD species arrival angle, as shown in Fig. 5, the effect of cavity shadowing on the reflectance is modeled in Fig. 9(a). As the reduction in deposition rate exceeds 46%, the reflectance band is shifted below 795 nm and the reflectance is reduced to below 90% and to as low as 10% on the lower face of sidewall reflector, becoming effectively transparent to light at the design wavelength over the lower region of the reflector.

However, the extended Bragg reflector design extends the high reflectance region over a wider area of the cavity sidewall, as modeled in Fig. 9(b). The thicker, shifted Bragg reflector provides high reflectance over the low portion of the sidewall. Only after the cavity shadowing reduces the deposition rate by 70% at the bottom of the cell is the sidewall reflectance reduced to less than 90%. An additional shifted Bragg reflector may be added to the design to extend the high reflectance region over the bottom section of the sidewall by using (14) twice to produce a double extended reflector.

In addition to high reflectivity, many applications, including atomic sensors, require the polarization state of the reflected light to be maintained. Fig. 10(a) models the polarization ellipticity of reflected light from a sidewall integrated conventional Bragg reflector. The incident light is considered to be ideally circularly polarized with an ellipticity of 45° . Over the high reflectance region, the reflected light remains circularly polarized. However, the polarization of the reflected light is not maintained at the edge of the high reflectance zone and over the low reflectance region. The polarization response complicates the response of the extended reflector, modeled in Fig. 10(b). At the transitions between the high reflectance regions provided by the conventional and the shifted Bragg reflectors, the reflected polarization may be seen to shift rapidly.

However, since Bragg reflectors maintain the state of circular polarization over the same spatial region in which high reflectance is achieved, the majority of optical power incident over the surface of the reflector will be returned maintaining a state of circular polar-

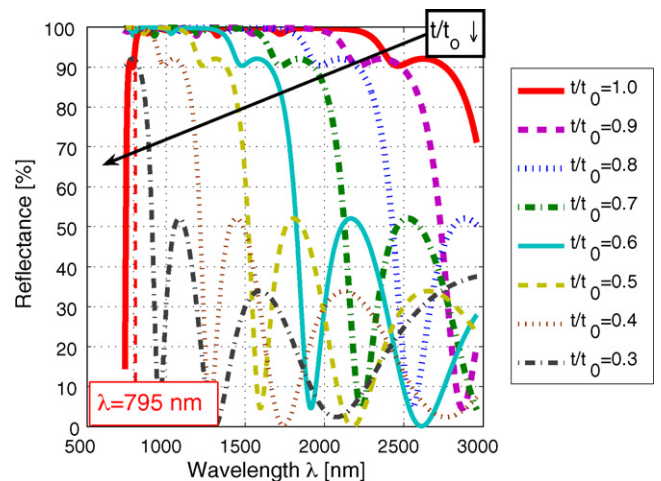


Fig. 7. Reflectance robustness under thinning due to extended spectral bandwidth.

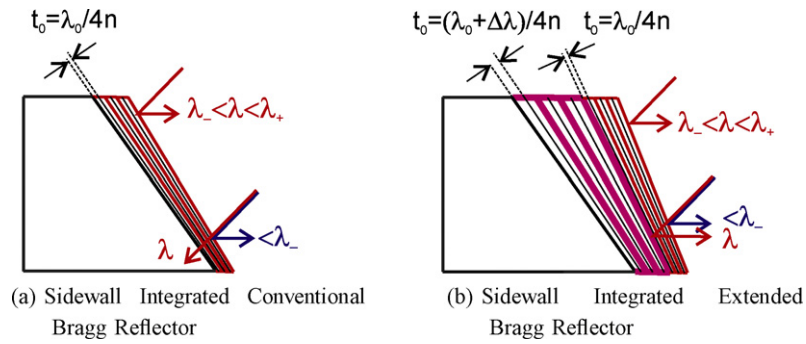


Fig. 8. Conventional vs. extended Bragg reflector design for robustness to deposition shadowing. (a) Sidewall integrated conventional Bragg reflector. (b) Sidewall integrated extended Bragg reflector.

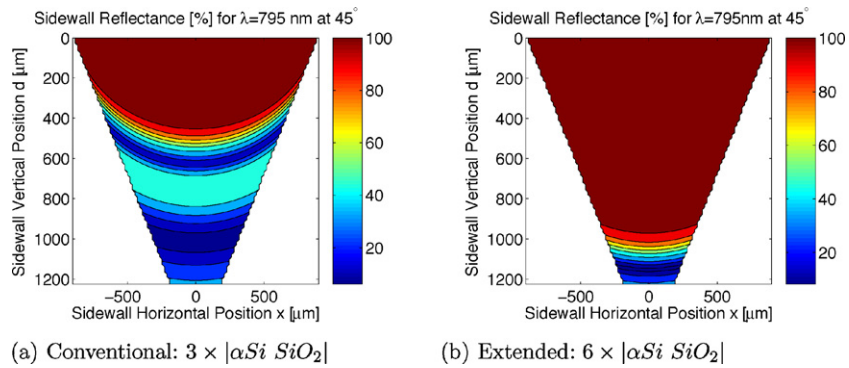


Fig. 9. Modeled reflectance under cavity deposition shadowing for sidewall PECVD Bragg reflectors ($L_0 = 1.8$ mm, $\alpha = 54.7^\circ$). (a) Conventional: $3 \times |\alpha Si SiO_2|$. (b) Extended: $6 \times |\alpha Si SiO_2|$.

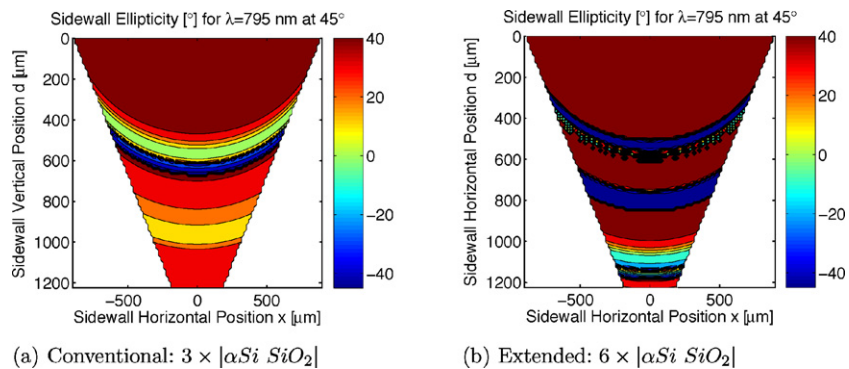


Fig. 10. Modeled reflected ellipticity of circularly polarized light under cavity deposition shadowing for sidewall PECVD Bragg reflectors ($L_0 = 1.8$ mm, $\alpha = 54.7^\circ$). (a) Conventional: $3 \times |\alpha Si SiO_2|$. (b) Extended: $6 \times |\alpha Si SiO_2|$.

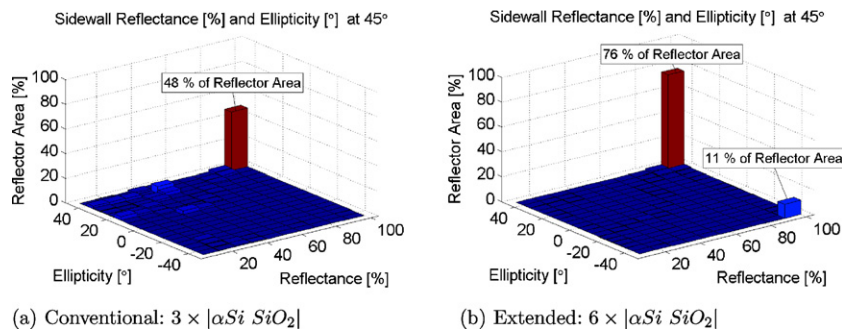


Fig. 11. Modeled reflectance and ellipticity distribution under cavity deposition shadowing for sidewall PECVD Bragg reflectors ($\lambda = 795$ nm, $L_0 = 1.8$ mm, $\alpha = 54.7^\circ$). (a) Conventional: $3 \times |\alpha Si SiO_2|$. (b) Extended: $6 \times |\alpha Si SiO_2|$.

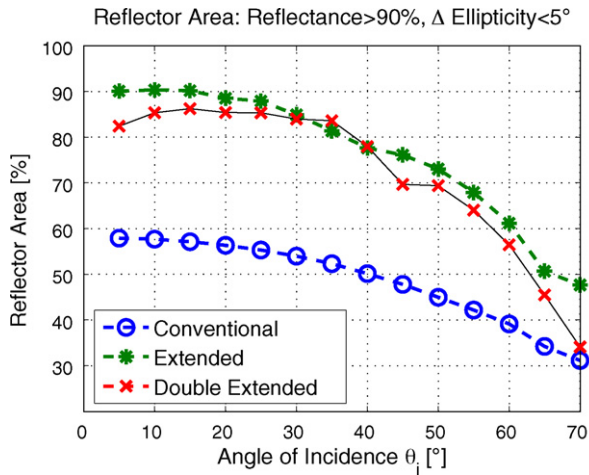


Fig. 12. Reflector design comparison of sidewall area achieving high reflectance and low circular polarization ellipticity change under cavity deposition shadowing for sidewall PECVD Bragg reflectors ($\lambda = 795$ nm, $L_0 = 1.8$ mm, $\alpha = 54.7^\circ$).

ization. Fig. 11(a) shows the distribution of the modeled reflectance and ellipticity response for a conventional sidewall reflector, which shows that 48% of the reflector has better than 90% reflectance and changes the polarization ellipticity by less than 5° , indicating that better than 43% of the optical power will return maintaining circular polarization. The extended Bragg reflector design, modeled in Fig. 11(b), shows that 76% of the reflector area achieved reflectance better than 90% with less than 5° change in ellipticity, increasing the returned optical power maintaining circular polarization to better than 68%. However, the extended reflector design introduces a significant component over 11% of the reflector area with reflectivity over 90% but with a polarization response of opposite handedness. Such response is expected over the region of the sidewall where the reflection band edges of the two individual (conventional and shifted) Bragg reflectors are nearly equal to the target wavelength.

The reflectance and polarization responses of Bragg reflectors are generally sensitive to the angle of incidence. Fig. 12 compares the conventional and extended Bragg reflector designs for the fractional spatial area of the sidewall reflector that maintains both high reflectance greater than 90% and low change in circular polarization ellipticity less than 5° . At angles of incidence approaching normal, the extended reflector design improves the performance from below 60% for the conventional Bragg design to better than 90% of the sidewall reflector. As the angle of incidence increases, the performance degrades due to increased ellipticity change and decreased reflector bandwidth. However, the extended reflector shows improved performance for angles of incidence up to 70° .

Also included for comparison is the double extended reflector that uses a total of three Bragg reflectors in series. Due to the polarization response, further extension of the Bragg reflector results in no increase in reflector surface achieving the desired high reflectance and circular polarization maintaining response. Due to this, such a double extended design is not expected to significantly improve the performance of the reflector.

4. Optimized cavity sidewall Bragg reflector implementation

The fabrication of a bulk micromachined cavity with an integrated Bragg reflector using a conventional, nonoptimized design has been described previously [4]. The current effort uses an iden-

tical fabrication process but with an optimized extended $|\alpha\text{Si SiO}_2|$ Bragg reflector design. Briefly, the cavities are wet etched in a 45% KOH + 5% IPA solution at 80°C into 1 mm thick double side polished silicon wafers using an LPCVD silicon nitride hardmask patterned with square windows to expose the $\langle 111 \rangle$ crystalline planes at 54.7° . The αSi and SiO_2 PECVD thin films are deposited under continuous vacuum onto the cavity surfaces at 250°C using a PlasmaTherm 790 [14]. For the SiO_2 film deposition, the chamber pressure is 900 mTorr, power is 25 W, and the reactant gas flow rates are N_2 at 150 sccm, N_2O at 50 sccm, and SiH_4 at 2.75 sccm. For the αSi film deposition, the chamber pressure is 980 mTorr, power is 30 W, and the reactant gas flow rates are N_2 at 75 sccm, and N_2O at 4 sccm.

The optimized, extended reflector is composed of two six layer Bragg reflectors in series with a total of 12 alternating αSi and SiO_2 thin films, as shown in Fig. 13. From Section 2.4, a thin film Bragg reflector composed of $|\alpha\text{Si SiO}_2|$ layer pairs with $\alpha = 54.7^\circ$ and target wavelength $\lambda = 795$ nm, a planar deposition wavelength is estimated to be $\lambda_0^\perp = 1480$ nm. The wavelength λ_0^\perp is used to establish the deposition time to achieve the thin film thickness from (1) for the deposition rates in any particular PECVD system. This yields the optimized planar deposition thicknesses of the upper (thinner) six layers of αSi and SiO_2 to be 90 and 240 nm, respectively. Using (9), upon deposition onto the sidewall of the cavity, the thicknesses of the films are expected to be reduced by 30%, which yields estimated sidewall thicknesses t_0 of 60 nm and 170 nm, respectively. These thinner layers provide high reflectance over the upper section of the cell.

For the $|\alpha\text{Si SiO}_2|$ film pair Bragg reflector, the shifted reflector is optimally designed with $\lambda_0^S = 1.8\lambda_0$, increasing the thickness of each of the layers of the shifted reflector by 80% over the design of the original, conventional Bragg reflector. The extended reflector extends high reflectance over the lower section of the cell by use of six thicker layers of αSi and SiO_2 thin films with planar deposition thicknesses 170 nm and 430 nm, sidewall thicknesses t_0 of 120 and 300 nm. These layers were implemented underneath (substrate side) of the optimal conventional Bragg reflector.

The double extended reflector design uses an additional Bragg reflector to further extend the high reflectance zone by use of three Bragg reflectors in series, as shown in Fig. 14. Each of the shifted Bragg reflectors may be observed. This includes the conventional, optimized Bragg reflector designed that provides high reflectance at the design wavelength at the top of the sidewall, the first extended Bragg reflector for high reflectance over the middle of the sidewall, and the second extended for high reflectance over the bottom of the sidewall. Each reflector may be thought to act as a short, medium and long wavelength reflector, respec-

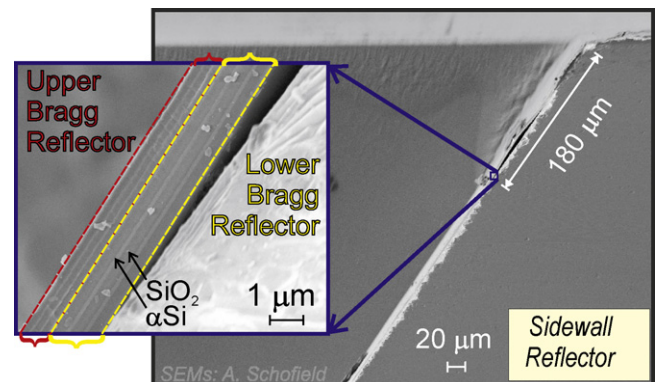


Fig. 13. Cavity sidewall integrated extended Bragg reflector cross section (SEMs courtesy A. Schofield).

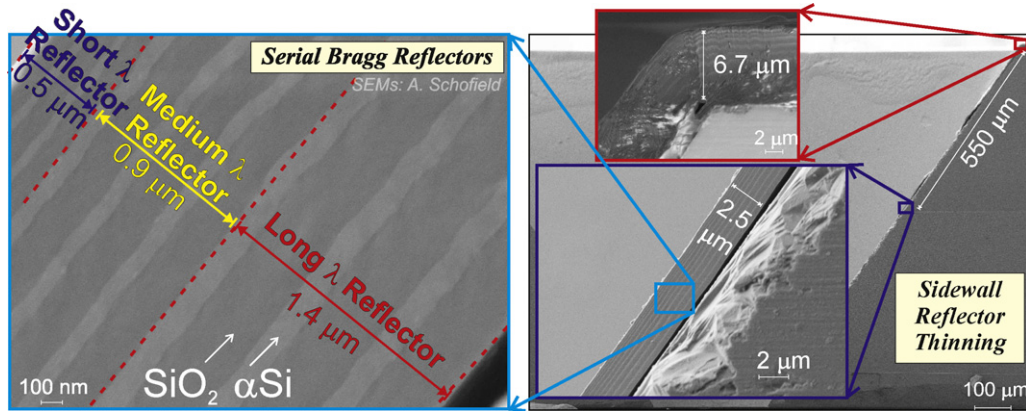


Fig. 14. Cavity sidewall integrated double extended Bragg reflector cross section (SEMs courtesy A. Schofield).

tively, although the design is to optimize the reflectance at the single design wavelength. The thickness ratios between each Bragg reflector are $1.4/0.9 \approx 0.9/0.5 \approx 1.8 \pm 0.2$, which follows from the design according to (14).

The thinning due to cavity shadowing is readily apparent in the cross section of the thin film structure in Fig. 14. The total thickness of the extended Bragg reflector decreases from $6.7 \mu\text{m}$ for perpendicular deposition at the top of the cell to $2.5 \mu\text{m}$ only $d = 550 \mu\text{m}$ down the cell sidewall. Evaluating (9) for the change in deposition from perpendicular to sidewall indicates reduction to 70% thickness. A further reduction at $550 \mu\text{m}$ down the sidewall face to 55% of the thickness at the top of the sidewall is expected from the modeling illustrated in Fig. 5. Taken together, a total thinning of the reflector structure to 39% of the original planar deposition thickness is expected. The observed thinning of $2.5 \mu\text{m}/6.7 \mu\text{m} = 0.37$ matches to within 2%.

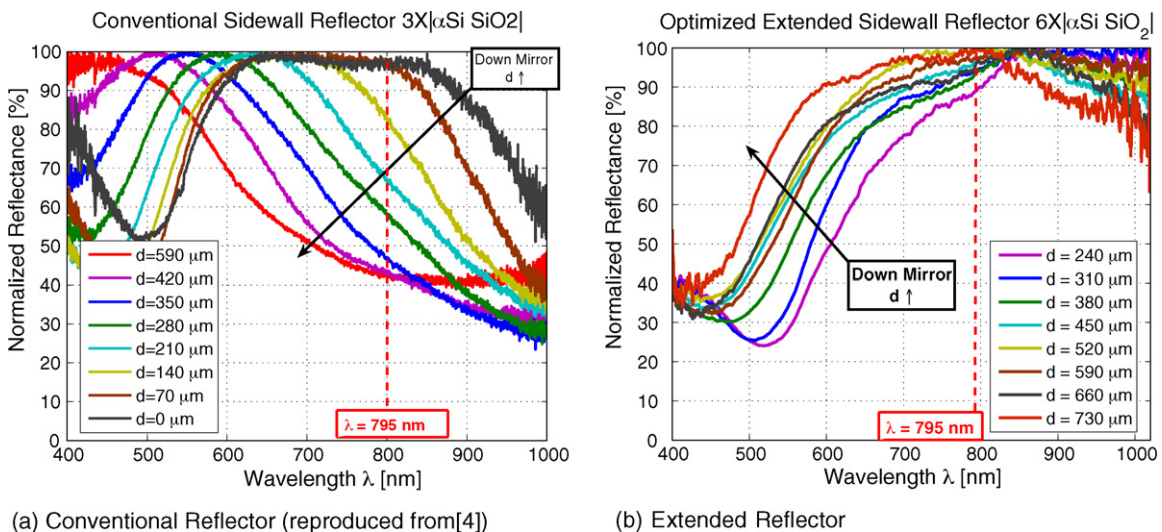
5. Extended Bragg reflector characterization

5.1. Reflector bandwidth

The reflectance bandwidth of the reflector face of a cell with an integrated 12-layer single extended Bragg reflector faces was characterized by using an Ocean Optics USB2000 [14] spectrometer

with a reflection probe coupled to an broadband LS-1 [14] tungsten halogen light source, as shown in Fig. 15(b). Due to the finite spot size of the reflectance probe light and the rapid spectral variation with sidewall position, the changes in reflectance at the lower edge of the reflectance bands are shallower than expected from the characteristic Bragg reflectance response. However, the wavelength limits of the reflection band may be extracted from the half power reflection point. The expected shift in the reflectance bandwidth due to cavity shadowing is observed in the shift to lower wavelengths of the lower bandwidth limit. Due to the extended reflectance bandwidth, the design wavelength of $\lambda = 795 \text{ nm}$ is not traversed by the upper reflectance bandwidth limit for over $d = 730 \mu\text{m}$ down the cavity sidewall.

The lower reflectance bandwidth of the extended reflector ($\lambda_{-, ext.}$) is compared to the experimentally observed upper ($\lambda_{+, conv.}$) and lower ($\lambda_{-, conv.}$) wavelength limits for the previously fabricated six layer conventional reflector not optimized for sidewall deposition (from Fig. 15(a), previously presented in [4]) in Fig. 16. Overlaid are the analytically projected reflectance bandwidths assuming PECVD cavity shadowing expected from (5). The optimized reflector is demonstrated to maintain high reflectance at 795 nm over more than 85% of the cavity sidewall, compared to less than 20% for the previously fabricated conventional Bragg reflector.



(a) Conventional Reflector (reproduced from [4])

(b) Extended Reflector

Fig. 15. Experimental comparison of conventional and extended sidewall integrated multilayer reflectors. (a) Conventional reflector (reproduced from [4]). (b) Extended reflector.

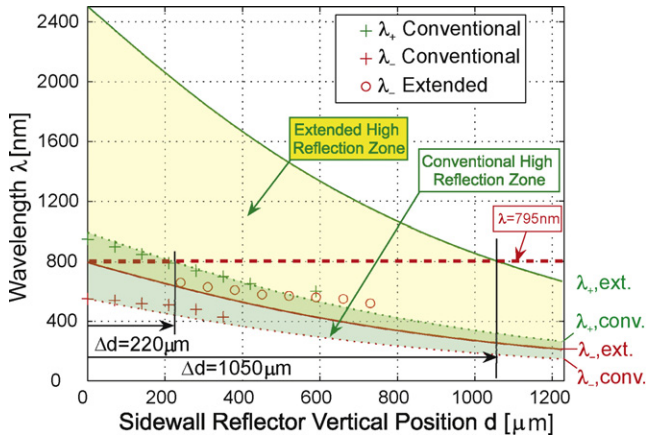


Fig. 16. Conventional (Fig. 15(a)) vs. optimally designed extended (Fig. 15(b)) Bragg reflectors for use at $\lambda = 795$ nm in micromachined reflector cell.

5.2. Sidewall reflectance

The performance of the reflector cell with integrated multi-layer reflector is demonstrated at 795 nm by mounting a sample on a rotation stage from which the circularly polarized collimated beam from a ULM VCSEL [14] is directed via the sidewall reflectors into a Thorlabs PAX polarimeter [14], as shown in Fig. 17. The VCSEL beam is passed through an appropriately oriented half wave plate, then a quarter wave plate to circularly polarize the VCSEL beam, which is linearly polarized upon emission from the VCSEL. Changes in the ellipticity are monitored to indicate the change in polarization state due to reflection from the reflector surface.

The performance of the sidewall reflector is tested with a single reflection from a cleaved half-cell. The reflectance from the sidewall integrated extended Bragg reflector is shown in Fig. 18. The single extended sidewall integrated reflector is demonstrated to have a reflectance better than 80% for incident angles up to 45°, as shown in Fig. 18(a). The change in ellipticity from circular polarization over the same angle of incidence range is observed to be less than 4°. Note that the decrease in reflection and increase in change in ellipticity with angle of incidence is predicted by the numerical models presented in Section 3 and summarized in Fig. 12. For the extended Bragg reflector design, as the angle of incidence increases, the reflector surface area achieving high reflectance and low change in ellipticity is predicted to decrease from 90% at normal incidence to 60% at 60° incidence, which is the same as the pattern observed experimentally.

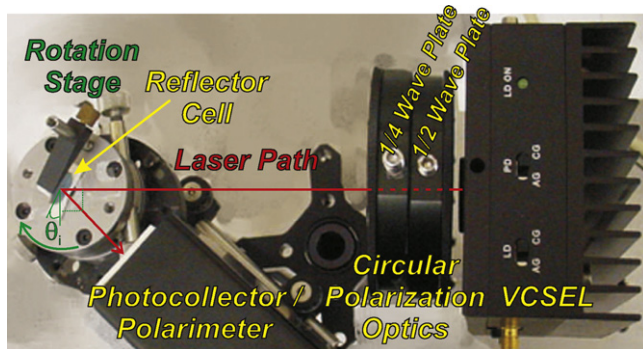


Fig. 17. Experimental stage for return reflection characterization of micromachined reflector cell.

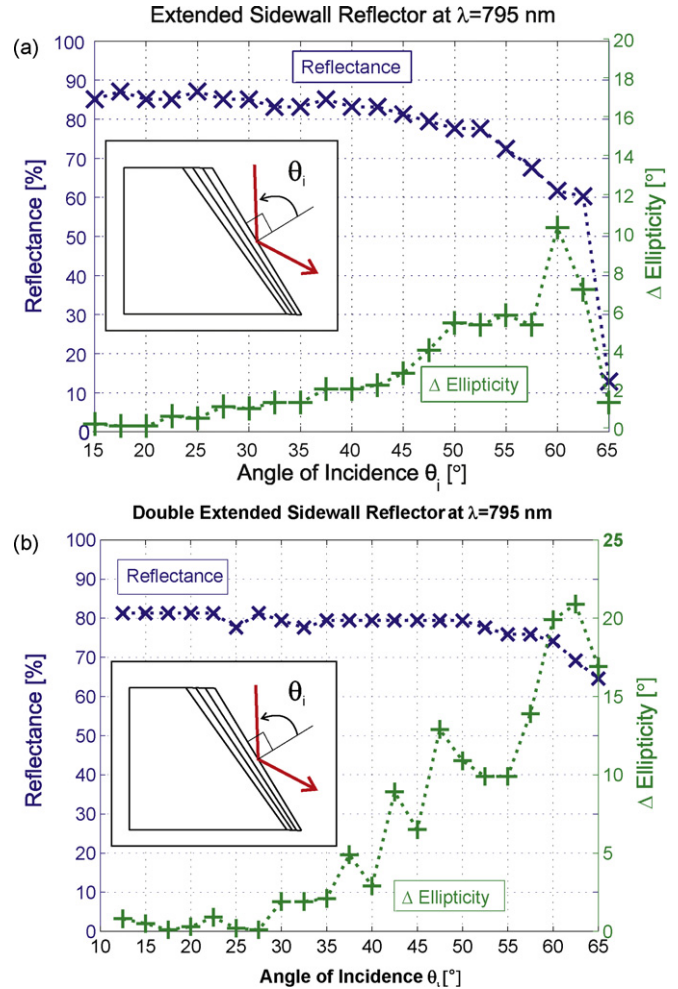


Fig. 18. Experimental reflection characterization of the extended and double extended Bragg sidewall reflector. (a) Single extended reflector. (b) Double extended reflector.

The double extended Bragg reflector design is observed to not improved the performance, as shown in Fig. 18(b). Although the reflectance performance is comparable to that of the single extended reflector, the ellipticity changes more rapidly with increasing angle of incidence with the returned ellipticity change exceeding 5° at incident angle over 40°. Such behavior is expected from the numerical models in which regions of high ellipticity change are expected to decrease the reflector performance at higher angles of incidence.

Low loss optical power return maintaining polarization is needed for atomic MEMS vapor cell applications over a range of angles of low incidence to the cavity aperture to admit the divergent interrogation beam from a VCSEL [15]. Use of a divergent beams to interrogate a micromachined vapor cell with integrated reflectors has been proposed for atomic magnetometers and gyroscopes [16].

The performance of the reflector cavity using a single extended Bragg reflector for multiple reflections is tested using the return reflection from two of the sidewalls of the complete cell. The return reflection from a complete reflector cavity is shown in Fig. 19. Return reflection from using two sidewalls of the complete cell is shown to achieve optical losses of less than -2 dB over incident angles to the plane of the cavity aperture from 5° to 30°. Over the same range of angles of incidence, the circular polarization is maintained to $\pm 2^\circ$ of ellipticity.

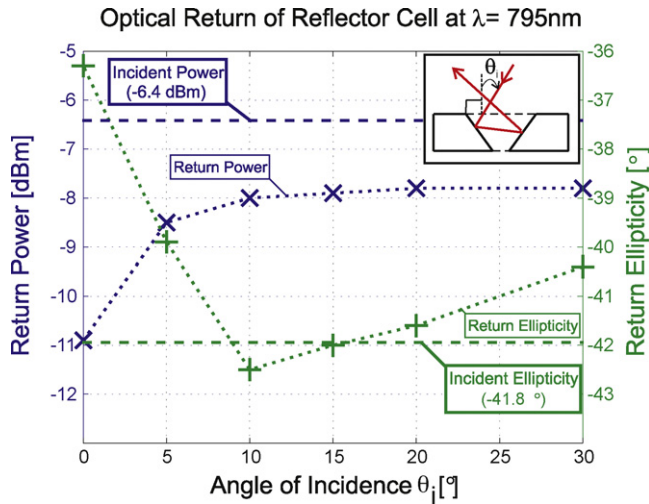


Fig. 19. Experimental return reflection characterization of the extended Bragg reflector cell.

6. Conclusions

An optimized design procedure for the integration of multilayer PECVD reflectors onto the sidewalls of bulk micromachined cavities has been introduced and experimentally demonstrated. The reflector design technique allows for the fabrication of reflector cells with improved optical return performance. This procedure optimizes the reflectance bandwidth for the cavity geometry to maintain high reflectance under deposition nonuniformities caused by deposition shadowing. A design for an extended reflectance band was introduced by use of two shifted Bragg reflectors in series. The design was shown to be effective in maintaining high reflection at the D_1 absorption wavelength of ^{87}Rb despite nonuniformities in excess of 70% for optical return applications. The fabricated cell was characterized to be able to return light at 795 nm with losses less than 2 dB while maintaining the polarization ellipticity of circular polarized light to $\pm 2^\circ$. In this paper we demonstrate an effective technique for the integration of multilayer reflectors with nonplanar microdevices, such as on the sidewalls of deeply micromachined cavities. This work paves the way for the introduction of high performance optics into atomic MEMS sensors and other optical MEMS with nontrivial geometries.

Acknowledgements

The authors thank the staff of the Integrated Nanosystems Research Facility (INRF) for fabrication support and A. Schofield for micrograph assistance. Numerical optical calculations were done by use of the Electromagnetic Waves and Antennas MATLAB package by S.J. Orfanidis [14]. This work was supported in part by the Defense Advanced Research Projects Agency (DARPA) Navigation-Grade Integrated Micro Gyroscopes (NGIMG) program and is a partial contribution of the National Institute of Standards and Technology (NIST), an agency of the US government, and is not subject to copyright.

References

- [1] D. Younger, L. Lust, D. Carlson, S. Lu, L. Forner, H. Chanhvongsak, T. Stark, A manufacturable chip-scale atomic clock, *Transducers'07 & Eurosensors XXI: The 14th International Conference on Solid-State Sensors and Actuators and Microsystems*, 2007.
- [2] L.A. Liew, S. Knappe, J. Moreland, H. Robinson, L. Hollberg, J. Kitching, Micro-fabricated alkali atom vapor cells, *Appl. Phys. Lett.* 84 (2004) 2694.
- [3] S. Knappe, V. Gerginov, P.D.D. Schwindt, V. Shah, H.G. Robinson, L. Hollberg, J. Kitching, Atomic vapor cells for chip-scale atomic clocks with improved long-term frequency stability, *Opt. Lett.* 30 (2005) 351–353.
- [4] M.A. Perez, U. Nguyen, S. Knappe, E.A. Donley, J. Kitching, A.M. Shkel, Rubidium vapor cell with integrated Bragg reflectors for compact atomic MEMS, *Sens. Actuators A*, in preparation.
- [5] L. Martinu, D. Poitras, Plasma deposition of optical films and coatings: a review, *J. Vacuum Sci. Technol. A: Vacuum, Surf. Films* 18 (2000) 2619–2645.
- [6] A. Adams, Plasma deposition of inorganic films, *Solid State Technol.* 26 (1983) 135–139.
- [7] V. Gottschalch, R. Schmidt, B.R.D. Pudis, S. Hardt, J. Kvietkova, G. Wagner, R. Franzheld, Plasma-enhanced chemical vapor deposition of $\text{SiO}_x/\text{SiN}_x$ Bragg reflectors, *Thin Solid Films* 416 (2002) 224–232.
- [8] M. Perez, J. Kitching, A. Shkel, Robust optical design of angled multilayer dielectric mirrors optimized for rubidium vapor cell return reflection, in: *Proceedings of the Hilton Head Workshop 2008: A Solid-State Sensors, Actuators and Microsystems Workshop (Transducers Foundation)*, 2008.
- [9] H.A. Macleod, *Thin-Film Optical Filters*, 3rd ed., Institute of Physics Publishing, Bristol–Philadelphia, 2001.
- [10] E.D. Palik, *Handbook of Optical Constants of Solids*, vol. 1, Elsevier, 1998.
- [11] D. Babic, S. Corzine, Analytic expressions for the reflection delay, penetration depth, and absorptance of quarter-wave dielectric mirrors, *IEEE J. Quantum Electron.* 28 (1992) 514–524.
- [12] A.F. Turner, P.W. Baumeister, Multilayer mirrors with high reflectance over an extended spectral region, *Appl. Opt.* 5 (1966) 69–76.
- [13] O.S. Heavens, H.M. Liddell, Staggered broad-band reflecting multilayers, *Appl. Opt.* 5 (1966) 373–376.
- [14] Products or companies named here are cited only in the interested of complete scientific description, and neither constitute nor imply endorsement by NIST or by the US government.
- [15] E. Hodby, E.A. Donley, J. Kitching, Differential atomic magnetometry based on a diverging laser beam, *Appl. Phys. Lett.* 91 (2007) 011109 (pages 3).
- [16] J. Kitching, E. Donley, E. Hodby, A.M. Shkel, E.J. Eklund, Compact atomic magnetometer and gyroscope based on a diverging laser beam (UC OTA Case # 2008–002), 2008.